Characterisation of the topography of metal additive surface features with different measurement technologies

Characterisation of the topography of metal additive surface features with different measurement technologies

Nicola Senin[1,2], Adam Thompson[1] and Richard Leach[1]
[1]Manufacturing Metrology Team, Faculty of Engineering, The University of Nottingham, NG7 2RD, UK
[2]Department of Engineering, University of Perugia, 06125, Italy

Abstract. The challenges of measuring the surface topography of metallic surfaces produced by additive manufacturing are investigated. The differences between measurements made using various optical and non-optical technologies, including confocal and focus-variation microscopy, coherence scanning interferometry and X-ray computed tomography, are examined. As opposed to concentrating on differences which may arise through computing surface texture parameters from measured topography datasets, comparative analysis is performed focussing on investigation of the quality of the topographic reconstruction of a series of surface features. The investigation is carried out by considering the typical surface features of a metal powder-bed fusion process: weld tracks, weld ripples, attached particles and surface recesses. Results show that no single measurement technology provides a completely reliable rendition of the topographic features that characterise the metal powder-bed fusion process. However, through analysis of measurement discrepancies, light can be shed on where instruments are more susceptible to error, and why differences between measurements occur. The results presented in this work increase the understanding of the behaviour and performance of areal topography measurement, and thus promote the development of improved surface characterisation pipelines.

Key words: surface metrology, three-dimensional topographic features, additive manufacturing, metal powder-bed fusion.

1. Introduction

An array of technologies are now available for capturing the three-dimensional (3D) topographic formations on surfaces at micrometric and sub-micrometric scales [1]. Optical technologies, particularly including confocal microscopy [2,3], coherence scanning interferometry [4,5] and focus variation microscopy [6,7], are capable of returning dense point-based samplings of a surface in relatively short measurement times. In addition to the optical methods, X-ray computed tomography (XCT) has recently been found capable of capturing topographic information at micrometric scales, provided the spatial frequencies of interest are within the reconstructed volumetric dataset [8–11]. Significant obstacles in the measurements are, however, yet to be overcome, particularly in assessment of the accuracy of such measurement technologies when capturing topographic detail of highly complex and irregular surfaces [8,12].

Metal additive manufacturing (AM) represents a relatively new tool in the field of advanced manufacturing, beneficial to an array of potential applications, but numerous barriers exist to the technology's increased industrial adoption. Particularly, in relation to the verification of parts produced by metal AM processes, a requirement for further research in accurate, 3D topography measurement has been identified [13,14]. Topography measurement is a fundamental means towards a better understanding of surface appearance and functional properties, such as fatigue performance, tribological properties and heat transfer behaviour. In particular, 3D topography measurement can capture detailed

information about how topographic formations are generated and later evolve during processing, post-processing and the functional life of the part [15]. However, metal additive surfaces are often highly complex and irregular (as shown in the example scanning electron and optical microscope images of a top surface, in figure 1), and measurements often show significant discrepancies between measurement technologies [10]; an issue which is particularly true for the powder-bed fusion (PBF) family of metal additive processes. The focus of this work is the measurement of the top surface of a metal PBF layer, as the top surface carries a signature of the physical interactions taking place during fabrication of the layer. The side surfaces of a metal PBF part also present interesting properties, as they are the result of the multiple layers accumulating during the build process. However, information pertaining to layer fabrication, as carried by side surfaces, is typically more difficult to unravel and so side surfaces they are not considered in this work.

The topography of the surface of a build layer is the result of complex interactions between the input material and an energy source scanning over the layer (typically a laser or electron beam). This interaction involves the formation of melt pools, the ejection on particles and drastic thermal gradients [16,17]. Surface topography is typically dominated by weld tracks, resulting from the fusion and subsequent solidification of a melt pool [18], which impart a strong texture directionality indicative of the laser (or electron) beam path. At smaller scales, weld tracks are covered by chevron-shaped ripples, indicating the beam scanning direction, and may feature smaller-scale thermal cracks and areas of local oxidisation. Throughout weld tracks, high aspect-ratio singularities are observable, typically consisting of deep recesses or sphere-like protrusions. Recesses may result from incomplete seams between weld tracks, balling phenomena (i.e. discontinuities of the track itself) or, at smaller scales, open micro-porosity [19–21]. Sphere-like protrusions are formed either from unmelted or partially-melted powder particles (appearing alone or in clusters), or spatter particles, i.e. molten material ejected from the melt pool during beam traversal, that impact the nearby surface during solidification [19]. As the metal PBF surface is the result of multiple melting and re-melting phenomena, involving the current layer as well as a variable number of layers underneath, multiple, larger-scale, wave-like components affect the final appearance of the top surface. Examples of these features are visible in figure 1a, where the shape of the weld tracks is affected by an undulation component with wavelength on the order of magnitude of a few hundreds of μm, presumably due to the irregularities of the layer underneath where, as a result of the scanning strategy implemented in the build, tracks lie at an angle of 67.5° to the current layer. The resulting partially random, partially deterministic topography of the top surface of the current layer, usually forms a recognisable pattern, i.e. the "fingerprint" of PBF technology [16,17].

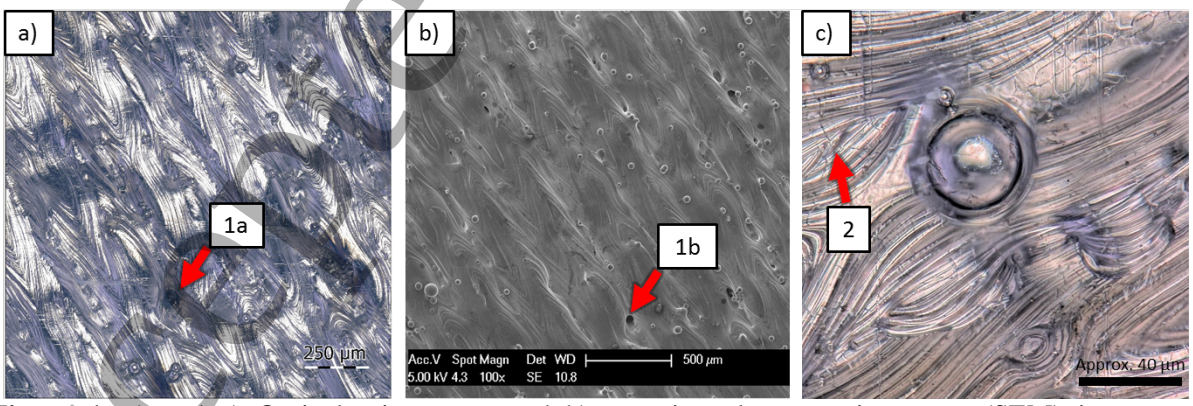

Figure 1. a) and c) Optical microscope and b) scanning electron microscope (SEM) images of topographic features typical of a Ti6Al4V metal laser PBF top surface, manufactured using a Renishaw AM250 equipped with a pulsed fibre laser. Arrows 1a and 1b point to the same example surface recess in optical and SEM images respectively, while arrow 2 indicates local cracking in a higher resolution

image. Straight vertical and horizontal scratches also visible in the image were caused by contact stylus measurements performed as part of a wider experimental campaign.

The metal PBF topography is a challenge for areal topography measurement. High slopes, variable aspect-ratios, alternation between dark and overly bright regions (e.g. deep recesses and the tops of smoother regions of particles and weld tracks), as well as non-uniform optical properties as a result of local oxidisation and/or micro-roughness effects, cause the main issues faced by optical measurement technologies [22]. XCT measurement is subject to an equally complex series of non-optical challenges which affect the spatial resolution of the measurement [9], as well as the procedure used to determine a surface from XCT data [8]. In recent work by the authors [10], discrepancies between measurements made on metal PBF surfaces using a number of areal topography instruments were quantified, and measurement discrepancies were found to be of the same order of magnitude as the size of localised topographic features captured by the measurement process. The comparison performed in this work mainly focused on examination of how changes in reconstructed topographies ultimately affected the results of the computation of texture parameters commonly used in industrial specifications (i.e. ISO 4287 [23] profile parameters and ISO 25178-2 [24] areal parameters). However, when the measurement concerned is performed with an interest in localised surface features, then the investigation of how local topography is reconstructed through different measurement technologies is of fundamental importance. In this case, particularly for PBF surfaces, assessments of how different technologies reconstruct quasi-spherical shapes, deep recesses, abrupt height or slope variations and smaller-scale features, such as weld track ripples and/or thermal cracks, is of significant interest.

2. Methodology

In this work, a region of interest (ROI) on a Ti6Al4V metal PBF surface was inspected using three optical areal topography instruments: a focus variation (FV) microscope, a confocal microscope (CM) and a coherence scanning interferometer (CSI). A fourth dataset was obtained by surface extraction from a volumetric reconstruction of data acquired using X-ray computed tomography (XCT). Multiple smaller regions were digitally extracted from the four topography datasets, representing examples of relevant metal PBF surface features (particles, recesses, ripples and weld tracks). Individual feature topographies were aligned in the same coordinate system and cropped to the same field of view (FOV) for comparison purposes, using a custom, dedicated geometric relocation procedure (see section 2.3). For visual comparison, datasets were levelled to a consistent mean height and rendered with artificial colouring based on a shared colour palette, mapped to the same range of heights, in order to provide a visual indication of local similarities and differences. For quantitative comparison, local height discrepancies between pairs of aligned topographies were computed.

2.1. Examined sample

The ROI used is a square of (1.5 × 1.5) mm in size, taken from the top surface of a (20 × 20 × 20) mm cube artefact, manufactured from Ti6Al4V using a Renishaw AM250 laser PBF machine, from a CAD model of a cube with nominally flat faces. The ROI is located at a corner of the artefact surface, so that the cube edges could be used as alignment references by which to compare topography measurements. The cube was not post-processed other than light cleaning, so as to still carry clear signs of the process fingerprint of the laser PBF process. Because of the abundance of particles and other singularities, the artefact used in this study possibly represents a slightly more challenging measurement scenario than a typical laser PBF surface.

2.2. Measurement setups

The measurement setups used in this comparison were chosen so as to cover an area large enough to form a valid assessment of the laser PBF surface, whilst considering total measurement time. Higher resolutions would have been possible, but would have taken a long time to process, while generating large, difficult-to-handle datasets.

Areal topography measurement setups (where LR is lateral resolution): CM, 20× objective lens (NA 0.6, FOV 0.64 mm × 0.64 mm, LR LR-pixel 0.63 μm, LR-optical 0.32 μm); CSI, 20× at 1× zoom (NA 0.40, FOV 0.42 mm × 0.42 mm, LR-pixel 0.41 μm, LR-optical 0.68 μm); FV, 20× (NA 0.40, FOV 0.81 mm × 0.81 mm, LR-pixel 0.44 μm, LR-optical 0.68 μm, LR-contrast 3.00 μm, ring light illumination). LR-pixel refers to the pixel width of the detector used by each instrument, LR-optical refers the calculated Sparrow optical limit of each instrument and LR-contrast refers specifically to the distance from the centre of each pixel used by the FV instrument to compute local contrast; selected during the measurement. All datasets were obtained by stitching of multiple images, performed in the instrument manufacturer's proprietary software. In each optical measurement setup, additional magnifications were considered but ultimately discarded; being either too low resolution to capture relevant topographic details, or too time consuming to achieve equivalent lateral coverage of the ROI and resulting in excessively large datasets. All datasets from optical areal topography measurement instruments (FV, CSI and CM) were obtained in raw form, as digital elevation models (DEMs – height values on a regular grid). Optical images were obtained by focus-stacking with at 200× magnification and SEM images were obtained at 61× magnification, in secondary electron mode.

X-ray measurement setup: geometric magnification of 44.1×, leading to voxel size of 4.53 μm, 3142 X-ray projections formed by averaging two frames per projection acquired using an X-ray tube voltage of 145 kV and current of 66 μA. A 0.25 mm copper X-ray pre-filter was used. XCT volumetric data were reconstructed in the manufacturer's proprietary software, using a second order beam hardening correction. Surfaces were determined in VGStudio MAX 2.2 by Volume Graphics [25], using a surface determination algorithm based on the local maximum gradient method [26]. The surface was exported as a triangulated mesh and raster scanned into a height map within the surface metrology software MountainsMap by DigitalSurf [27] at a spatial resolution automatically determined by MountainsMap to match the point density of the original triangulated mesh (2.87 μm).

2.3. Data processing

Void values in the DEMs (present in all the datasets except those from the XCT) were replaced by weighted linear interpolation of all the available valid neighbours (each weight being inversely proportional to distance between the reference neighbour and the interpolated point). For alignment, datasets were converted into triangulated meshes by Delaunay triangulation [28]. Alignment was implemented by using custom Matlab code developed by the authors and consisted of an initial marker-based coarse alignment (markers manually placed by an operator and alignment obtained via resolution of the absolute orientation problem [29]), followed by fine alignment via application of the iterative closest point method [30]. After alignment, triangulated meshes were reconverted into DEMs by projection of vertical rays along the rows and columns of a regular x,y grid (referred to as raster scanning in this work), with a custom x,y sampling grid of 0.5 μm spacing (a resolution higher than the highest in the original datasets, to avoid information loss, while at the same time achieving resolution parity in the final datasets) and finally cropped to the same lateral extents.

The assessment of local height discrepancy was implemented between pairs of aligned DEMs, where one was always the CSI dataset, used as a reference. Discrepancy was quantified as differences between local height values, computed at each x,y position of the aligned DEMs.

3. Results and discussion

3.1. Full ROI

The complete ROIs are shown in figure 2. While the reconstructed topography appears relatively consistent between measurements, closer visual inspection yields topographic differences, in particular in relation to CSI and CM datasets featuring more content at high spatial frequencies, though this content

is noisier in the CM case. Conversely, CSI contained more unmeasured points (voids), not shown in figure 2 because voids were filled by interpolation of valid neighbours.

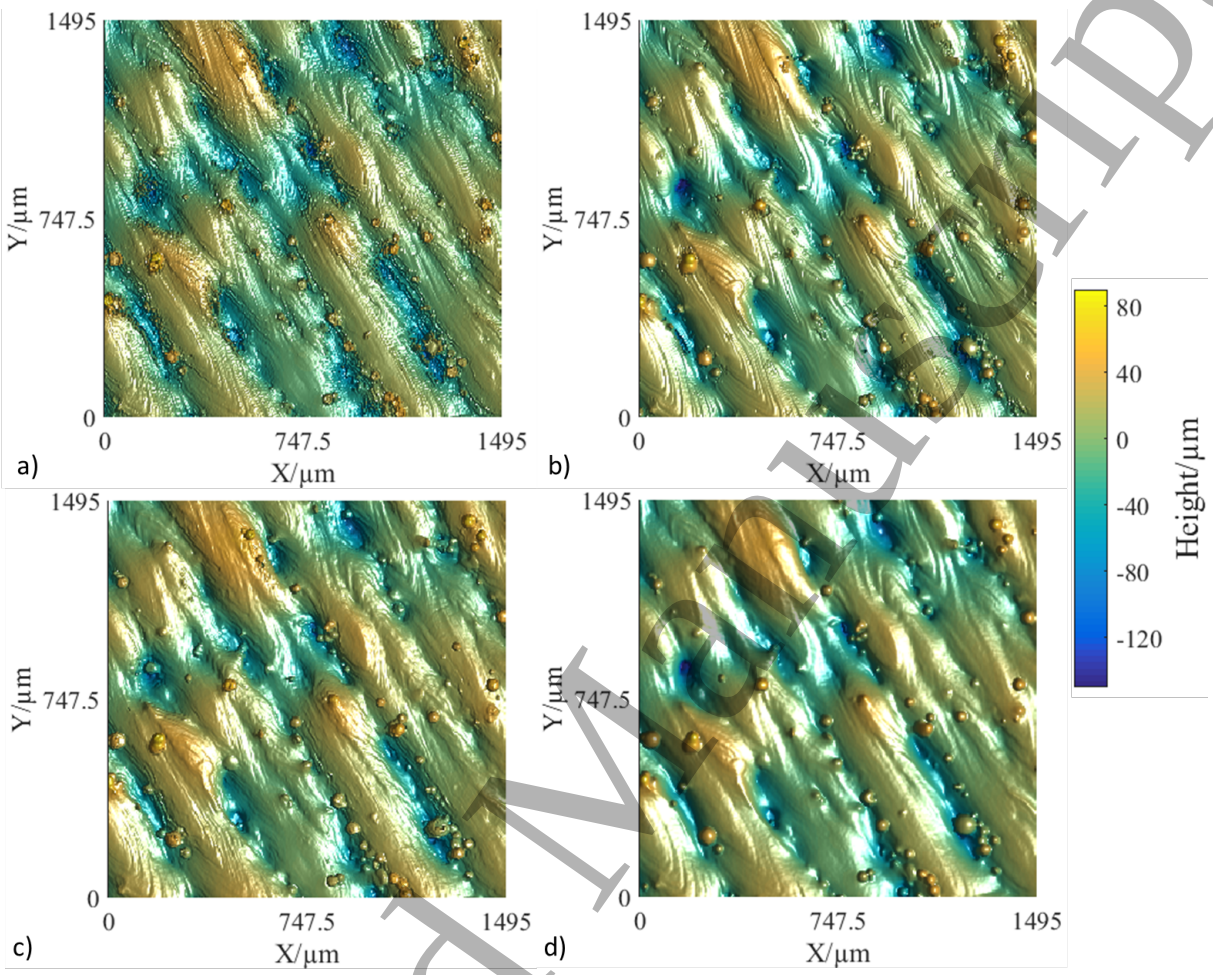

Figure 2 Complete topography datasets: a) CM, b) CSI, c) FV and d) XCT.

3.2. Attached particles

The topographies of two example attached particles are shown in figure 3. The process of aligning and computing local height differences, for the first particle shown in figure 3 is illustrated in figure 4, using the CSI and FV datasets as examples. In figure 5, local height discrepancy maps for the first particle shown in figure 3 are presented, using the CSI topography as a reference to better highlight the relationships between local height differences and topography.

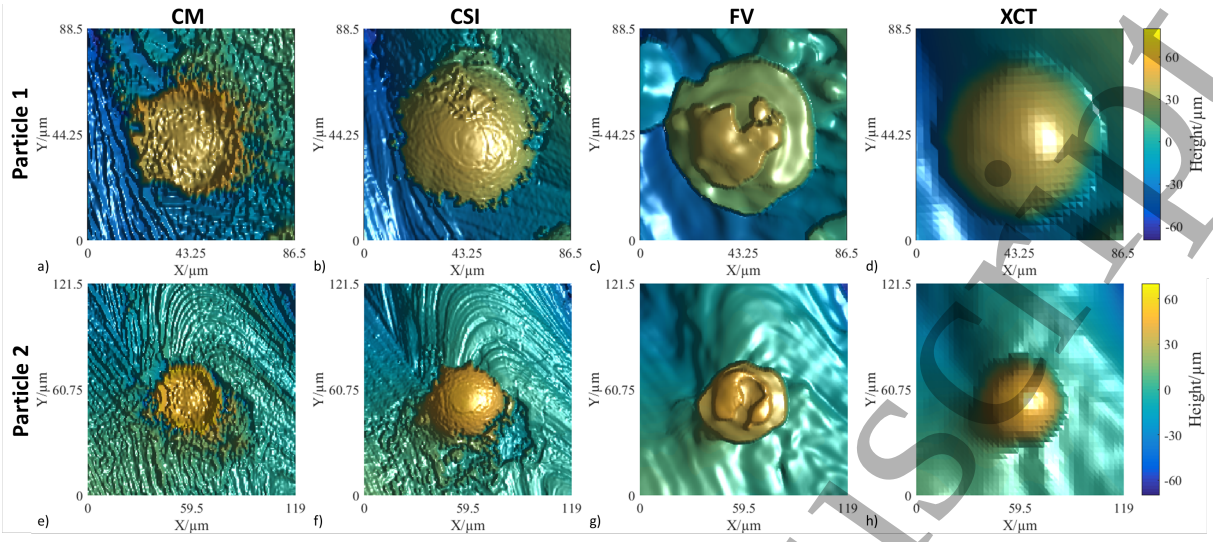

Figure 3 Topography of two attached particles. Two different window sizes were chosen, in the first case to highlight the particle, in the second case to additionally show a larger portion of the surrounding area.

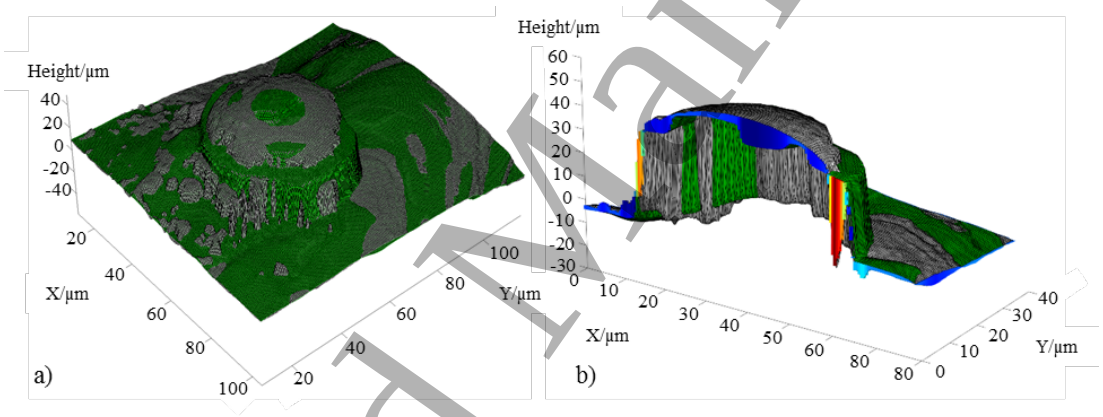

Figure 4. Computation of local height differences between CSI (grey) and FV (green) datasets; a) aligned meshes; b) cross-section of the particle and local height differences: blue and cyan indicate regions where the FV topography lies beneath the CSI topography, while orange and red represent where it lies above.

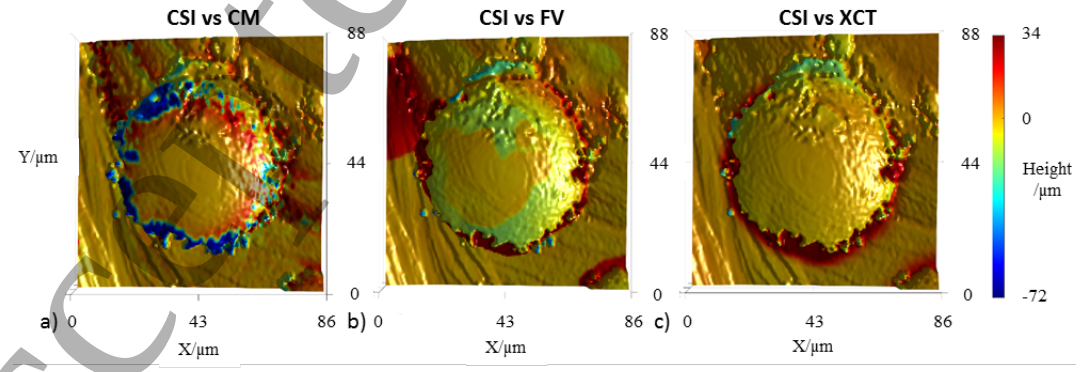

Figure 5. Local height discrepancy maps overlaid onto the CSI topography dataset. Colour is proportional to local (signed) height differences. The range of local height difference values is fixed for each feature instance, so that colours are comparable across images; the colour corresponding to zero

difference is highlighted in the colourbar (golden tint). Using CSI data as a reference, blue colouring indicates regions where the second measurement is lower, and red where it is higher.

Visual inspection of figure 3 and figure 5 reveals significant discrepancies between instruments. Although the technology is capable of recognising the presence of a protruding feature, CM is not in this instance able to correctly reconstruct the sphere-like nature of the particle (see also figure 1c as a reference). Nevertheless, feature boundaries are still clearly distinguishable, and make the particle discriminable from the immediate surroundings. This behaviour can be partially attributed to the known effects on CM data when measuring spherical geometry [31], but more research is required to establish the exact cause. CSI better captures the sphere-like nature of the particle, albeit with local irregularities that increase in frequency and amplitude with slope angle, as angles approach the measurable limit for the instrument [32]. FV operates by finding the probe-surface distance corresponding to maximum contrast within a region of observed image pixels, and thus experiences difficulty when a surface is locally very bright, very dark, or otherwise uniform because of its smoothness [7]. Sphere-like particles in metal PBF are often very smooth and highly reflective [19], thus forcing the FV technology to locally approximate height information by interpolation of information acquired from better contrasted, neighbouring points; leading to the plateau-like formation observable in figure 3. In general, for optical instruments, most discrepancies occur in regions containing high local slopes (see figure 5) as would be expected [12]. XCT reconstructions (figures 3d and 3h), despite being characterised by lower spatial resolution, are those in which the sphere-like nature of the particle is best captured due to the lack of optical or directional effects. As an aside, it should also be noted that the actual surface information extracted from XCT data is encoded as a full 3D triangulated mesh, which additionally makes XCT the only technology currently capable of capturing the re-entrant nature of the features (in this case, the underside of the sphere). For the purposes of this comparative analysis, however, the outputted triangulated mesh was converted into a DEM by raster scanning, in order to allow comparison to the optical datasets which natively return DEMs. Because of raster scanning, the re-entrant parts of the feature are lost in this comparison.

3.3. Recesses

Surface recesses are another highly challenging family of features that result in substantially different reconstructions dependent on measurement technology, due to the presence of high slopes and high aspect ratios. Further challenges in recess measurement result from the presence of clusters of agglomerated powder particles, located inside or surrounding recesses. Reconstructions from two example recesses are illustrated in figure 6, which shows particularly that two technologies, CM and FV, can fail to recognise a recess entirely, returning either high-frequency noise (CM, figures 6a and 6e), or even a protruded measurement artefact (FV, mostly evident in figure 6c, and to a lesser extent in figure 6g). The same result can be seen when examining the local height discrepancy maps overlaid onto the CSI dataset (figure 7) for the first recess shown in figure 6.

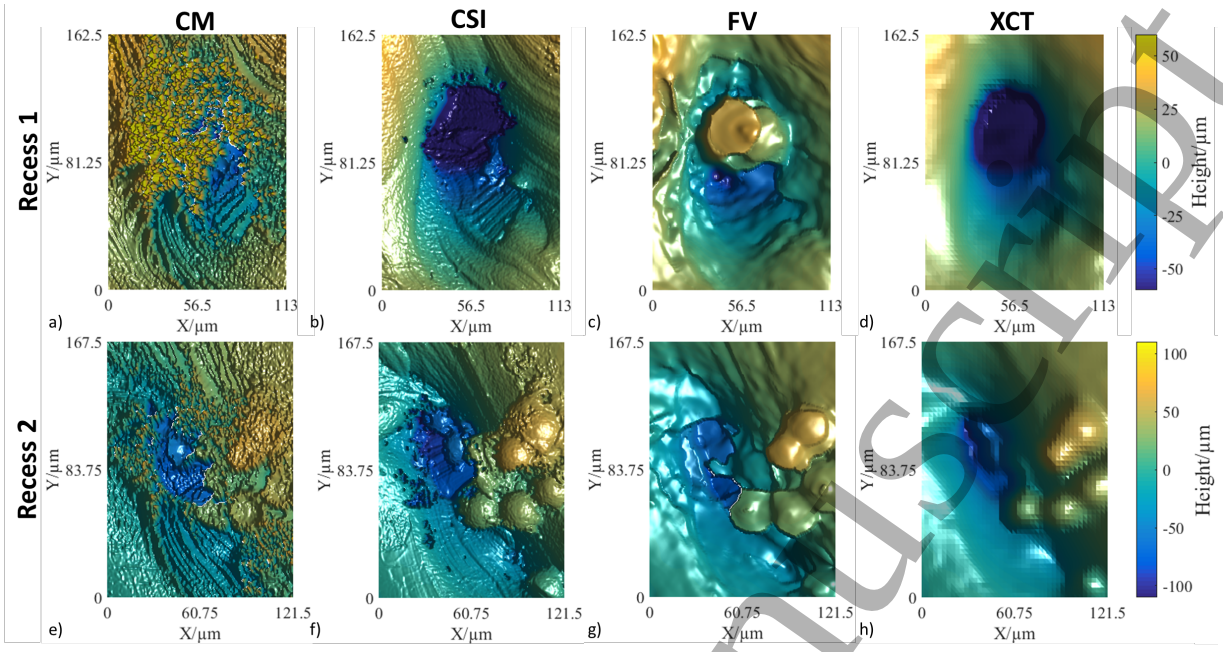

Figure 6. Reconstructions of two surface recesses. Two different window sizes were chosen in each case to highlight a single recess only, and a recess with surrounding particles.

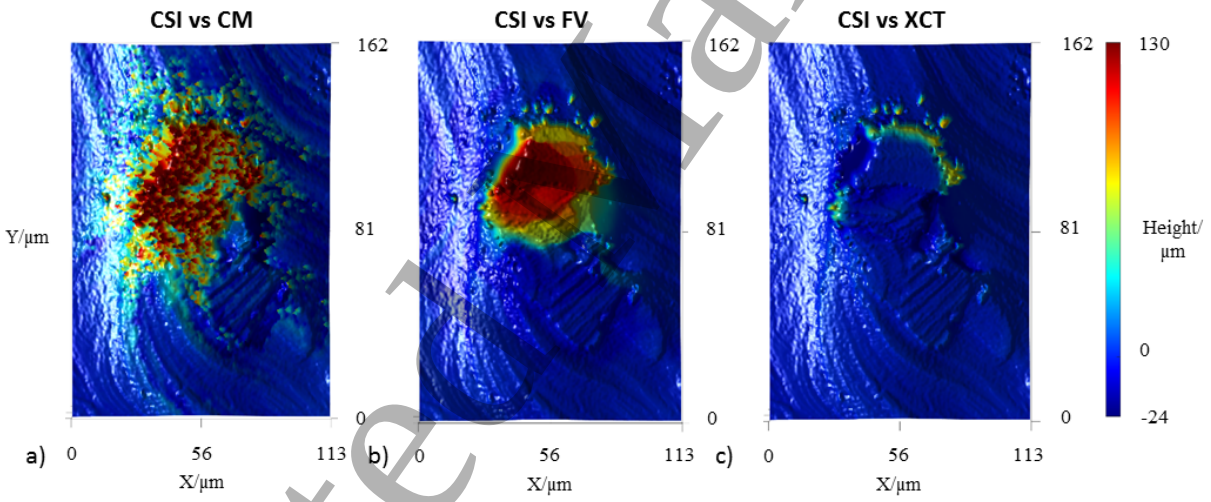

Figure 7. Local height discrepancy maps overlaid on the CSI topography dataset. Colour is proportional to local (signed) height difference. The range of local height difference values is fixed for each feature instance, so that colours are comparable across images; the colour corresponding to zero difference is highlighted in the colourbar (blue tint). Using CSI as a reference, red colouring indicates regions where the second measurement is higher.

Difficulties encountered when measuring recesses result from a scarcity of reflected light and multiple reflections from within recesses as a result of the presence of high slopes and aspect ratios, which are challenging for optical technologies (such effects are discussed in the instrument-specific chapters in [12]). It should be noted that despite the apparent superiority displayed in these results over CM and FV measurements, CSI measurements similarly suffer as a result of these issues; typically returning a greater number of non-measured points compared to other technologies (although, [33] suggests improvements to CSI technology that can mitigate some of these issues). This issue is not visible in figures 6 and 7 as non-measured points have been filled by interpolation of valid neighbours, for the purposes of accurate alignment. XCT measurements do not experience the difficulties faced by optical technologies, but the

intrinsically lower resolution of the measurement can result in filtering of smaller recesses from the data. Similar to the case of particles, XCT is also the only technology capable of capturing re-entrant features in recesses, such as sub-surface pore networks. Again, similarly to the particle case, due to the DEM conversion applied for comparison purposes in this work, such capability was not explored.

3.4. Weld ripples

When examining weld ripples (figure 8), significant differences between measurement technologies are apparent in regards to capture of high spatial frequency features.

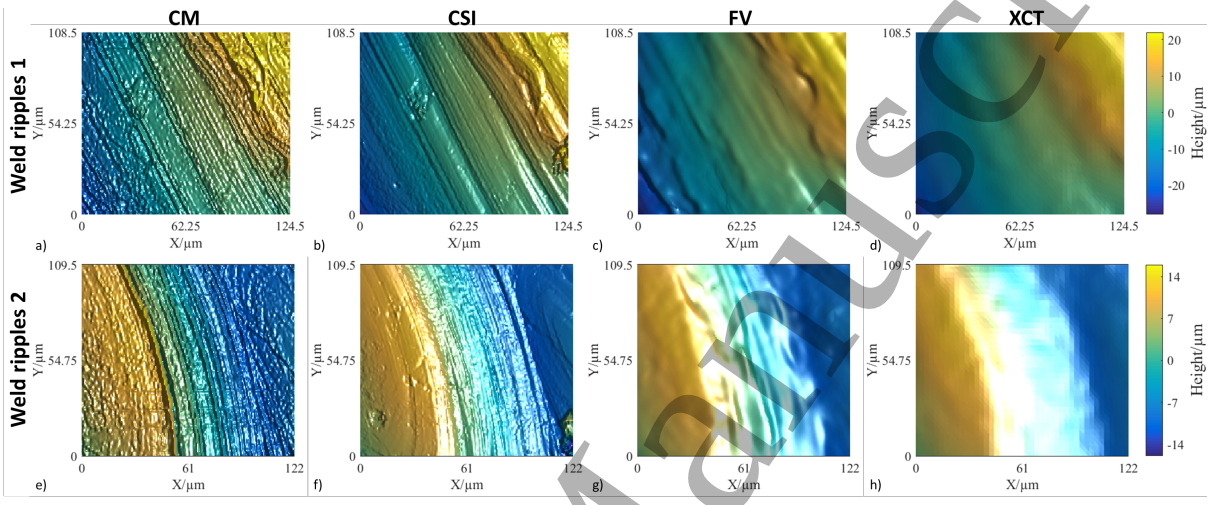

Figure 8. Reconstructed weld track ripples.

Both CM and CSI reconstructions of the same region return a high number of ripples, though the CM representation is more irregular. The presence of ripples is reported in the FV datasets to a lesser extent, where, while most of the small-scale detail is lost, it is still possible to discern larger-scale ripples. The majority of ripple information is lost in the XCT dataset. Differences across technologies are mostly due to the different lateral resolving power achievable through each technology (see the section 3.7 for further details). When investigating weld ripples, very little information can be gained from examination of local height discrepancy maps (figure 9), as differences between measurements are spread across the entire FOV. Nevertheless, by comparing the numeric values of the discrepancies (colourbar in figure 9) with those observed for the particles (figure 5) and recesses (figure 7) it can be noticed that the differences for the ripples are smaller, as a result of the lower aspect-ratios involved (colour maps are not directly comparable across figures because they are scaled on feature-specific intervals).

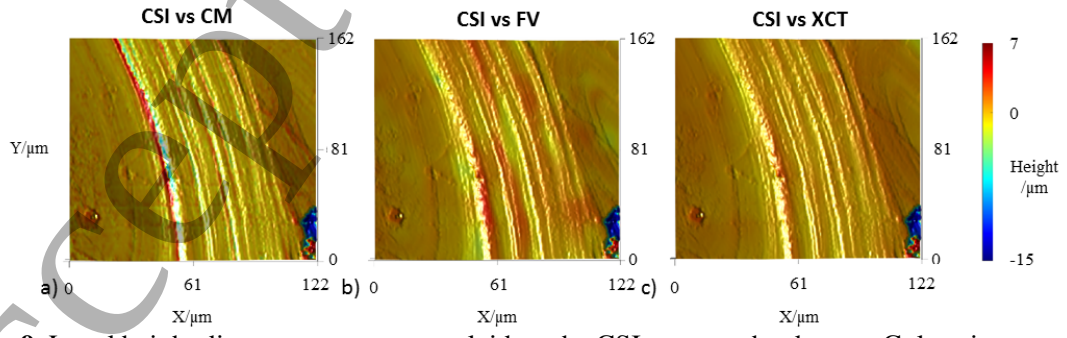

Figure 9. Local height discrepancy maps overlaid on the CSI topography dataset. Colour is proportional to local (signed) height difference. The range of local height difference values is fixed for each feature instance, so that colours are comparable across images; the colour corresponding to zero difference is

highlighted in the colourbar (golden tint). Using CSI as a reference, blue colouring indicates regions where the second measurement is lower, and red where it is higher.

3.5. Weld tracks

Weld tracks are complex, elongated protrusions, additionally comprising an assortment of ripples, particles, recesses, and other larger-scale wave-like components. Thus, when examining weld tracks, it is difficult to separate the underlying shape of the track from the smaller-scale features that cover its surface. Moreover, it is in itself often non-trivial to isolate an individual weld track, due to irregular boundaries and overlapping between multiple tracks [15]. One region approximately encompassing a pair of adjacent weld tracks is shown in figure 10a – 10d. Local height discrepancy maps (displayed in figure 10e – 10g) show that the greatest discrepancies between measurements are concentrated around the smaller-scale features discussed previously (particularly particles and recesses), while the larger-scale components of the topography have a more consistent appearance across measurements.

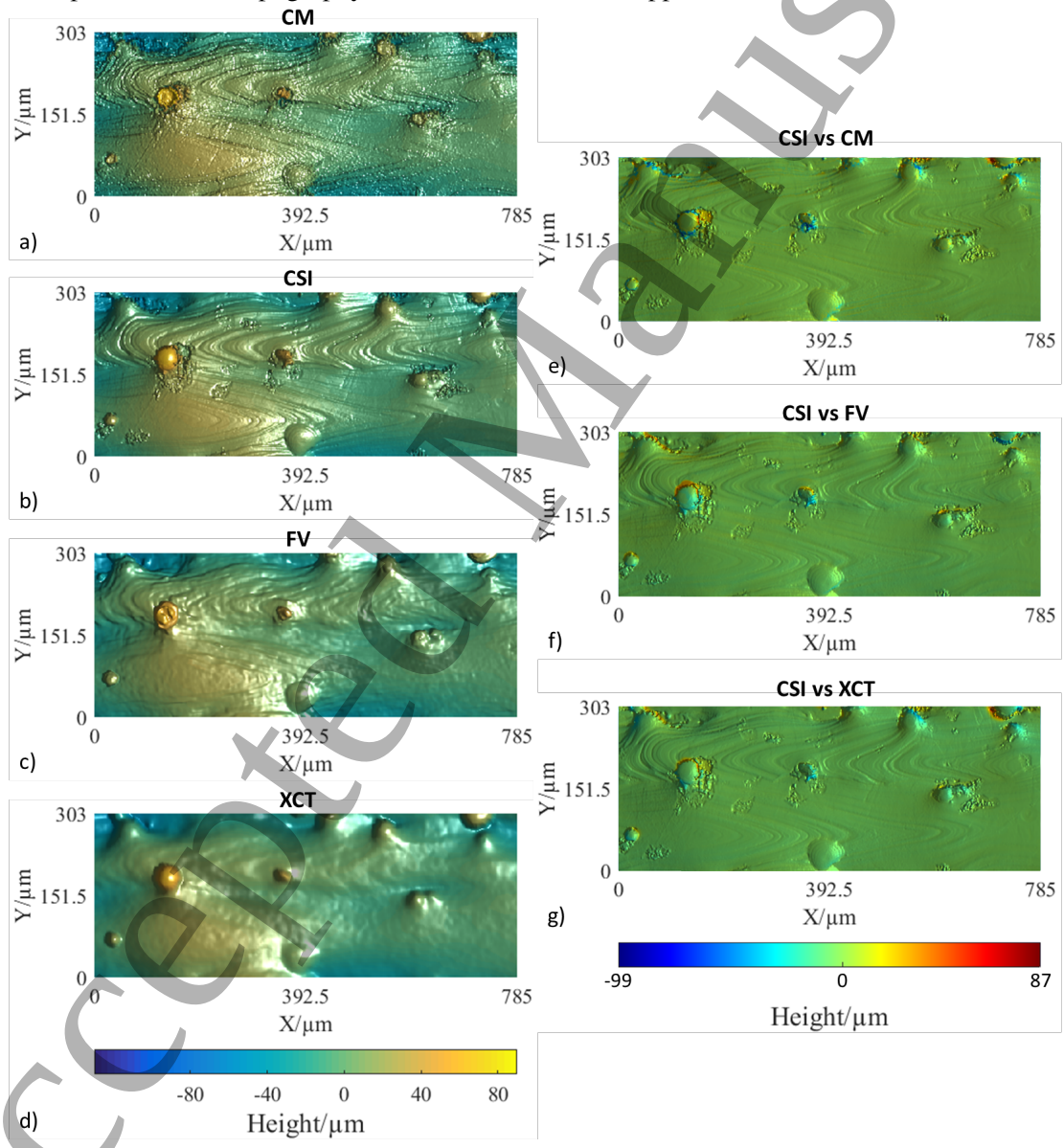

Figure 10. a) – d) Reconstructed weld tracks; e) – g) Local height discrepancy maps overlaid on the CSI dataset for the weld track region shown in figure 10. The range of local height difference values is fixed for each feature instance, so that colours are comparable across images; the colour corresponding to zero

difference is highlighted in the colourbar (green tint). Using CSI as a reference, blue colouring indicates regions where the second measurement is lower, and red where it is higher.

3.6. Distribution of local height differences within the FOV

The distribution of local height differences, again computed by using CSI as reference, can be investigated through the use of boxplots; those reported in figure 11 show the unsigned local height difference (the absolute value of the signed difference) for the features whose local height discrepancy maps have been shown in figures 5, (particle), 7 (recess), 9 (weld ripples) and 10 (weld track). The results show that the mean difference is similar across measurement types, and most of the differences are in the tails of the distributions, classified as outliers.

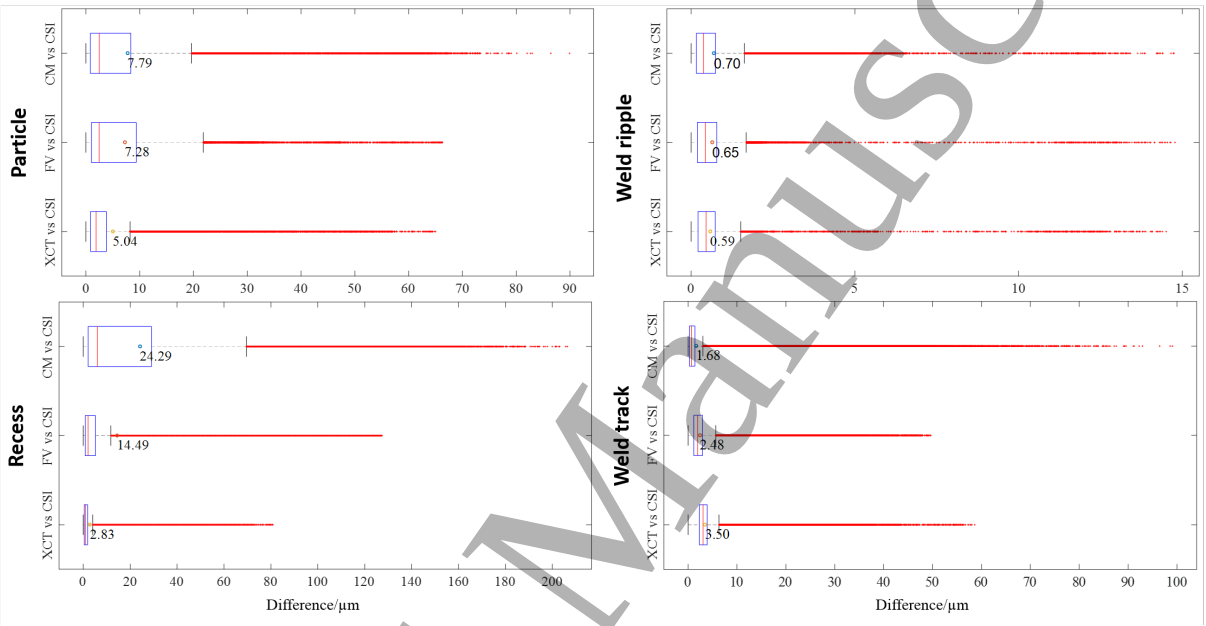

Figure 11. Boxplots illustrating the distribution of the unsigned local height difference for the four features whose local height discrepancy map is reported in figures 5, 7, 9 and 10. Each box plot reports the median, interquartile range, whiskers and outliers (red dots). Labelled circles indicate arithmetic means.

From a statistical viewpoint, differences between measurements are generally small (the median difference of each comparison is typically within the inter-quartile range of the others), and most of the significant differences appear as outliers. Provided the ROI is large enough to encompass a significant portion of the surface (e.g. multiple weld tracks), then the differences between measurements are less relevant as larger-scale topographic components are consistently captured across technologies. However, this scenario does not hold in the case where the FOV is occupied for the most part by difficult-to-measure topography. For example, a recess that occupies the majority of a FOV will lead to more significant non-outlier discrepancies, and so great care must be taken when assessing how much of the FOV is occupied by difficult-to-measure features, as the resulting consistency between instruments may be poor. For example, measurements made of the side surface of the same artefact used in this study as part of the wider experimental campaign yielded a dense array of attached particles (as reported elsewhere [15]), and by these results such a surface could represent the latter scenario discussed here.

3.7. Discussion

Differences between measurement results obtained through the application of different measurement technologies to the same topography are undeniable. For laser powder-bed fusion, the most significant differences relate to smaller-scale, high aspect ratio localised features.

If the purpose of the investigation is surface characterisation of large ROIs through computation of texture field parameters, then the discrepancies across technologies may be considered to have limited effects on the characterisation results (see [10] for an in-depth discussion on the effects of measurement technologies on texture parameters for additive surfaces). However, if the investigation is targeted at localised, smaller-scale features, (often the case in off-line metrology for manufacturing process development and optimisation), then the discrepancies between technologies become more significant, and so great care must be taken in the analysis and interpretation of measured data.

The results presented in this work point to high local slopes as a dominant factor in causing measurement discrepancies between optical technologies. More generally, high aspect-ratio features are the cause of many problems, as they often include a combination of high slopes and local variations in the amount of light returned to the detector (e.g. decreases in returned light relating to deep recesses, excesses in returned light from shiny, smooth protruded regions, such as attached particles). These problems do not affect XCT, both because the technology is not optical and because there is no unidirectional probing involved. Other problems do affect XCT though; this is a subject of current debate and ongoing investigation [8,34].

Moreover, as the majority of relevant differences observed in this work relate to the capability of instruments in reconstruction of small-scale topographic features, it is clear that measurement resolution factors in heavily. It is convenient to introduce the concept of lateral topographic resolution in measurement, as an indicator of a measurement technology's ability to resolve topographic detail at small scales on the surface plane. For the optical techniques (CM, CSI and FV) a combination of optical resolution (related to wavelength and the NA of the objective), pixel width (related to detector characteristics), and the raw-data processing pipeline used to obtain height information, leads to the final resolving power achievable by each technology. Data processing plays a particularly big part in the determination of lateral resolution. For example, FV requires a window of adjacent pixels to compute contrast (and thus compute local height) for any given pixel, which means that the heights of two adjacent pixels are not entirely independent (i.e. they are not fully resolved). This dependency means that the actual lateral resolution of a FV instrument is significantly poorer than that calculated by considering only pixel width and the optical resolution limit. Similarly, the ability of CSI and CM to resolve heights at given spatial frequencies (a term referred to as the "lateral period limit" in draft ISO specification standards [35,36]) needs to be determined (see [37] for a proposed method). For XCT, overall resolving power results from the resolution of the raw projections (a function of X-ray spot size and pixel width at the detector), how the X-ray images are processed and recombined to create a volumetric dataset and how the surface mesh is computed and extracted from the volumetric dataset [38]. In the configurations adopted for this work, CM and CSI were able to achieve sub-micrometric resolutions, while FV and XCT were limited to a few micrometres. The exact determination of resolving power as a function of measurement technology, process parameters and surface properties is in need for further investigation, and is subject of ongoing research (e.g. see [37]).

A note is reserved to the statistical significance of the observed results. Proper discrimination between measured topographies would imply a more thorough study of measurement-related error, in order to separate random and deterministic components, so as to make sure that observed differences are not entirely due to random chance. The problem of assessing the uncertainty associated with the topographic reconstruction is looming in this work along with the need for obtaining a better quantitative assessment of the systematic error components, hinted at in the previous sections. In previous work [10], the authors

have begun to address this issue through development of statistical models of measured topographies, but further effort is required in order to attain comprehensive models, in particular when modelling covariance (i.e. spatial correlation) between different points within the same field of view.

Finally, it is important to discuss how the results reported in this work can be generalised. The trends illustrated in this work have been consistently observed for multiple instances of particles, recesses, ripples and weld tracks. However, there remains a question regarding the portability of these results to different artefacts (different materials and/or different laser or electron beam PBF processes, and to the surfaces after post-processing). So far, similar operating conditions have led to consistent results: for example, the reconstructions of attached particles have consistently shown the same sets of issues, provided particles are nominally similar in size and shape. Other topographic features are more strongly dependent on set-up. For example, weld tracks may or may not be visible, depending on surface orientation, proximity to other features and the additive process used to fabricate the sample (e.g. laser against electron beam PBF, but also layer scanning parameters). As such, measurement technologies may behave slightly differently when applied to the measurement of other PBF surfaces, although they are expected to exhibit a similar metrological performance, consistent with the general conclusions illustrated earlier regarding the dependency on slope, aspect-ratio, etc.

Finally, it is worth considering the constant evolution of measurement technologies. As raw data processing within the instrument plays such a fundamental role in determining the final topographic reconstruction, it is expected that different results will be obtainable as new versions of measurement instruments enter the market. In such circumstances, the role of this work is to raise awareness about the fact that, at least currently, measurement error is far from negligible; in particular, in the case where accurate rendition of small-scale, local topographic features is required.

4. Conclusions

Quantitative comparison of topography data obtained by using different measurement technologies (CM, CSI, FV and XCT) shows that disagreement between reconstructions can be significant. This finding is particularly true in the case of smaller-scale features, where local height differences are found to be on the same order of magnitude as the features being measured. The reasons for such discrepancies can be found in the optical phenomena taking place in the interactions between measuring instruments and the specimen surface (for optical measurement technologies) and in an equivalent series of non-optical phenomena taking place in XCT measurement. Some of these phenomena have been discussed in this work, but significant research efforts are still needed and further work is in progress. At present, it can be stated that, for larger-scale topographic formations (i.e. formations that occupy a sizeable portion of the field of view), all measurement technologies return relatively consistent results. However, no topography reconstruction should be assumed to be reliable, regardless of measurement technology, particularly when the measured surface is as challenging as is often the case with metal PBF surfaces. Even in the case where the final goal is not to obtain an accurate rendition of individual topographic features, but instead to simply compute texture parameters, a better understanding of how and why each instrument reacts in the way it does to specific topographic formations is a requirement for results to be accepted and processed.

Finally, for no reason should any one of the illustrated measurement technologies be considered inferior or superior when measuring metal PBF surfaces. Results are heavily dependent on instrument make and model, current setup, and specific conditions related to the measured sample [33]. The primary message to be taken away from this work is that areal topography measurement of any form is affected by potentially large reconstruction errors, and that this should be seriously considered in any measurement campaign with an intention of accuracy.

Acknowledgements
The authors would like to thank Dr Peter de Groot and Dr Jack DiSciacca for their assistance in the acquisition of CSI data. AT and RKL would like to thank EPSRC (Grants EP/M008983/1 and EP/L01534X/1) and 3TRPD Ltd. for funding this work. NS and RKL would also like to thank the EC for supporting this work through the grant FP7-PEOPLE-MC 624770 METROSURF. The authors would like to thank DigitalSurf for providing the MountainsMap software and Prof. Chris Tuck (The University of Nottingham) for helpful discussions on the PBF process.

References
[1] Leach R K 2014 *Fundamental principles of engineering nanometrology* (Oxford, United Kingdom: Elsevier)
[2] ISO 25178-607:Under development Geometrical product specification (GPS) -- surface texture: areal -- part 607: nominal characteristics of non-contact (confocal microscopy) instruments (International Organisation for Standardization)
[3] Artigas R 2011 Imaging confocal microscopy In: *Optical measurement of surface topography* ed. R Leach (Berlin, Germany: Springer-Verlag) 237–86
[4] ISO 25178-604:2013 Geometrical product specifications (GPS) -- surface texture: areal -- part 604: nominal characteristics of non-contact (coherence scanning interferometry) instruments (International Organisation for Standardization)
[5] de Groot P 2011 Coherence scanning interferometry In: *Optical measurement of surface topography* ed. R Leach (Berlin, Germany: Springer-Verlag) 187–208
[6] ISO 25178-606:2015 Geometrical product specification (GPS) -- surface texture: areal -- part 606: nominal characteristics of non-contact (focus variation) instruments
[7] Helmli F 2011 Focus variation instruments In: *Optical measurement of surface topography* ed. R Leach (Berlin, Germany: Springer-Verlag) 131–66
[8] Townsend A, Pagani L, Scott P and Blunt L A 2017 Areal surface texture data extraction from x-ray computed tomography reconstructions of metal additively manufactured parts *Precis. Eng.* **48** 254-264
[9] Thompson A, Maskery I and Leach R K 2016 X-ray computed tomography for additive manufacturing: a review *Meas. Sci. Technol.* **27** 72001
[10] Thompson A, Senin N, Giusca C and Leach R 2017 Topography of selectively laser melted surfaces: a comparison of different measurement methods *Ann.CIRP*. **In Press**
[11] Stimpson C K, Snyder J C, Thole K A and Mongillo D 2016 Scaling Roughness Effects on Pressure Loss and Heat Transfer of Additively Manufactured Channels *J. Turbomach.* **139** 021003
[12] Leach R 2011 *Optical Measurement of Surface Topography* (Berlin, Germany: Springer-Verlag)
[13] Gao W, Zhang Y, Ramanujan D, Ramani K, Chen Y, Williams C B, Wang C C L, Shin Y C, Zhang S and Zavattieri P D 2015 The status, challenges, and future of additive manufacturing in engineering *Comput. Des.* **69** 65–89
[14] UK Additive Manufacturing Steering Group 2016 Additive Manufacturing UK September 2016 strategy update (Nottingham: UK Additive Manufacturing Steering Group)
[15] Townsend A, Senin N, Blunt L, Leach R K and Taylor J S 2016 Surface texture metrology for metal additive manufacturing: a review *Precis. Eng.* **46** 34–47
[16] Matthews M J, Guss G, Khairallah S A, Rubenchik A M, Depond P J and King W E 2016 Denudation of metal powder layers in laser powder bed fusion processes *Acta Mater.* **114** 33–42
[17] Khairallah S A, Anderson A T, Rubenchik A and King W E 2016 Laser powder-bed fusion additive manufacturing: Physics of complex melt flow and formation mechanisms of pores, spatter, and denudation zones *Acta Mater.* **108** 36–45
[18] Mazumder J 1991 Overview of melt dynamics in laser processing *Opt. Eng.* **30** 1208–19
[19] Simonelli M, Tuck C, Aboulkhair N T, Maskery I, Ashcroft I, Wildman R D and Hague R 2015 A study on the laser spatter and the oxidation reactions during selective laser melting of 316L stainless steel, Al-Si10-Mg, and Ti-6Al-4V *Metall. Mater. Trans. A Phys. Metall. Mater. Sci.* **46** 3842–51

[20] Tolochko N K, Mozzharov S E, Yadroitsev I A, Laoui T, Froyen L, Titov V I and Ignatiev M B 2004 Balling processes during selective laser treatment of powders *Rapid Prototyp. J.* **10** 78–87
[21] Gong H, Gu H, Zeng K, Dilip J J S, Pal D, Stucker B, Christiansen D, Beuth J and Lewandowski J J 2014 Melt pool characterization for selective laser melting of Ti-6Al-4V pre-alloyed powder *Solid Freeform Fabr. Symp. Proc.* (Austin, USA: University of Texas Austin) 256–67
[22] Leach R 2013 *Characterisation of areal surface texture* (Berlin: Springer-Verlag)
[23] ISO 4287:1997 Geometrical product specification (GPS) -- surface texture: profile method -- terms, definitions and surface texture parameters (International Organisation for Standardization)
[24] ISO 25178-2:2012 Geometrical product specifications (GPS) -- surface texture: areal -- part 2: terms, definitions and surface texture parameters (International Organisation for Standardization)
[25] Volume Graphics 2016 *VGStudio MAX* Available: https://www.volumegraphics.com/en/products/vgstudio-max.html (Accessed 11th May 2017)
[26] Lifton J J, Malcolm A A and McBride J W 2015 A simulation-based study on the influence of beam hardening in X-ray computed tomography for dimensional metrology *J. Xray. Sci. Technol.* **23** 65–82
[27] Digital Surf 2016 *Mountains® surface imaging & metrology software* Available: http://www.digitalsurf.com/en/mntkey.html (Accessed 11th May 2017)
[28] George P-L and Borouchaki H 1998 *Delaunay Triangulation and Meshing: Application to Finite Elements* (Oxford, UK: Butterworth-Heinemann)
[29] Horn B K P 1987 Closed-form solution of absolute orientation using unit quaternions *J. Opt. Soc. Am. A* **4** 629–42
[30] Besl P J and McKay N D 1992 A Method for Registration of 3D-Shapes *IEEE Trans. Pattern Anal. Mach. Intel.* **14** 239–56
[31] Weise W, Zinin P, Wilson T, Briggs G A D and Boseck S 1996 Imaging of spheres with the confocal scanning optical microscope *Opt. Lett.* **21** 1800–2
[32] Gao F, Leach R K, Petzing J and Coupland J M 2007 Surface measurement errors using commercial scanning white light interferometers *Meas. Sci. Technol.* **19** 15303
[33] Gomez C, Su R, Thompson A, DiSciacca J, Lawes S and Leach R 2017 Optimisation of surface measurement for metal additive manufacturing using coherence scanning interferometry *Opt. Eng.* **Under review**
[34] Townsend A, Pagani L, Blunt L, Scott P J and Jiang X 2017 Factors affecting the accuracy of areal surface texture data extraction from X-ray CT *Ann. CIRP.* **In Press**
[35] ISO 25178-3:2012 Geometrical product specifications (GPS) -- surface texture: areal -- part 3: specification operators (International Organisation for Standardization)
[36] ISO/FDIS 25178-600:2017 Geometrical product specifications (GPS) -- surface texture: areal -- part 600: metrological characteristics for areal-topography measuring methods (International Organisation for Standardization)
[37] Giusca C L and Leach R K 2013 Calibration of the scales of areal surface topography measuring instruments: part 3. Resolution *Meas. Sci. Technol.* **24** 105010
[38] Carmignato S, Pierobon A, Rampazzo P, Parisatto M and Savio E 2012 CT for industrial metrology-accuracy and structural resolution of CT dimensional measurements *Conf. Industrial Computed Tomography (iCT)* (Wels, Austria: Shaker Verlag)